A Model to Assess Zircaloy's Mechanical Property Changes Following a Transient Beyond Critical Heat Flux

Nathan Capps[1], Mackenzie Ridley[1], Samuel Bell[1], John Beale[2], David Schrire[3], Aaron Phillippe[4], Baris Sarikaya[5], Kan Sakamoto[6], and Nedim Cinbiz[1]

[1] Oak Ridge National Laboratory, 1 Bethel Valley Rd, Oak Ridge, TN 37830
[2]Electric Power Research Institute, 1300 West WT Harris Boulevard, Charlotte, NC 28262
[3] Electric Power Research Institute Contractor
[4]Southern Nuclear Company, 3535 Colonnade Pkwy, Birmingham, Alabama 35243
[5]Constellation Energy Generation, LLC, 200 Energy Way, Kennett Square, PA 19348
[6] Nippon Nuclear Fuel Development, Co., Ltd., 2163, Narita-Cho, Oarai-Machi, Higashi Ibaraki-Gun, Ibaraki-Ken 311-1313, Japan

ABSTRACT

Maintaining the integrity of nuclear fuel rods is essential for ensuring public health and safety in nuclear power generation. During reactor operation, this integrity is confirmed by demonstrating compliance with established regulatory acceptance criteria. For moderate-frequency events, such as limiting transients and anticipated operational occurrences (AOOs), the current fuel integrity criterion is based on preventing boiling transition. This criterion assumes that prevention of boiling transition will prevent excessive cladding heating and, thus, fuel failure during normal operations. While conservative, this approach places significant constraints on core design, fuel cycle economics, and a plant's ability to perform major power uprates, leading to suboptimal fuel utilization and inefficient carbon-free energy production. A more efficient approach could be achieved by revising the failure criterion to a material-specific limit rather than strictly preventing the boiling transition, since boiling transition *per se* is not a cause of fuel cladding failure. As a result, a new licensing framework based on material properties, termed *time-at-temperature* (t@T), is needed. This approach would allow for brief periods of post–critical heat flux operation during an AOO without compromising safety. Implementing the t@T licensing strategy requires a robust technical foundation in material properties, which must be established through comprehensive data collection on both unirradiated and irradiated fuel and cladding materials. This foundation would enable the development of a safety basis that ensures safe operation while providing greater flexibility and efficiency for reactor operation. This paper documents a thorough review of the available data to establish a baseline knowledge that can inform the development of cladding mechanical models, as well as identify experimental data gaps that need to be addressed in future research. Machine learning and data informatics were utilized to extract the importance of parameters on the t@T parameter. Industry tools were used to perform baseline analyses to define the relevant transient conditions for data analysis. The subsequent review successfully identified applicable experimental data, as well as sufficient data to evaluate changes in cladding mechanical properties following an AOO transient. Rather than developing new models, this work coupled existing irradiation annealing and recrystallization models to calculate changes in hardness, yield stress, and ultimate tensile stress following an AOO event. The findings from this review were summarized to highlight the experimental data needs required to fill remaining gaps and support the development of future t@T licensing methodologies.

1. Introduction

Most licensing regulations worldwide use dryout (DO) or departure from nucleate boiling (DNB) criteria to assess nuclear fuel cladding's ability to transfer heat during transient conditions. Specifically, DO and DNB criteria are commonly used to evaluate cladding heat transfer during an anticipated operational

Corresponding author*: cappsna@ornl.gov

occurrence (AOO), defining the point at which the critical heat flux (CHF) is exceeded. Fuel rods that exceed CHF—whether through DO or DNB—are considered to have failed, regardless of the duration or severity of the event [1,2]. This assumption is based on the significant change in coolant conditions that these phenomena cause, in which the transition from controlled boiling to steam (in the case of DO) or from nucleate boiling to film boiling (in the case of DNB) occurs. For high heat flux in a pressurized water reactor (PWR), the DNB creates a vapor or steam film that insulates the hot fuel rod, severely diminishing heat transfer. For boiling water reactors (BWRs), DO occurs with lower heat flux, where the vapor super heat is limited. As a result of DO, heat transfer is dominated by convective cooling to the vapor, but the resultant lower heat transfer coefficient leads to reduced cooling efficiency and rapid temperature increases in the cladding. This rapid rise in temperature may degrade the cladding material properties, resulting in potential for embrittlement if the cladding experiences a sufficiently high temperature for a sufficient duration.

In the U.S., the Nuclear Regulatory Commission (NRC) uses the DO and DNB criteria as conservative thresholds to prevent fuel failure when the CHF is exceeded [1]. However, because DO and DNB are thermal hydraulic phenomena, they do not fully describe the actual impact on the performance of the fuel rod materials. As a result, they are inherently conservative as failure criteria. A more accurate cladding failure criterion would consider not only the rate of temperature increase but also the duration of sustained high-temperature exposures. These factors are crucial for assessing how cladding's material properties evolve under transient conditions. Cladding mechanical property changes would then need to be taken into account when evaluating the continued safe operation of the fuel and, if necessary, post-transient handling of the fuel.

Many AOOs involve a reactor trip, which limits the amount of heat that must be removed by the coolant. Although these AOOs, especially those with short durations in post-DNB conditions, are relatively rare, international experience with reactor operation in DO conditions suggests that the current, strict DO criteria may be overly conservative [1-20]. Adopting a fuel integrity criterion that allows for short durations in post-DNB conditions could provide additional operational margins [2]. Such a modification would enable improvements in several areas, such as increased plant operational flexibility, fuel conditioning, quicker power level adjustments, enhanced fuel cycle economics with more efficient core designs, and better-optimized BWR control rod sequencing. Generic assessments indicate the value of these changes on the order of 1M to 1.5M USD per cycle for BWRs [4]. Specifically, the development of a new limit to replace the current operating limit minimum critical power ratio (OLMCPR) is being explored for BWRs. Substituting the OLMCPR with a thermomechanical limit based on time-at-temperature (t@T) could offer sufficient margin to uprate many high-power-density plants that are currently constrained by OLMCPR. The potential benefits for PWRs are more complex. PWR AOOs are generally more severe than those in BWRs, and the effective use of additional margin may depend on a variety of factors. Nevertheless, PWRs could see a potential ~5% increase in power output or peaking factors, which, when combined with successful burnup extension and higher enrichment levels, can further enhance performance [4].

This paper presents a review of available data on AOO events and related analyses to determine the appropriate conditions for evaluating Zircaloy cladding performance following such events. This review is followed by an examination of existing data on Zircaloy behavior under steady-state and transient annealing conditions, with the goal of assessing how simulated AOO transients affect the evolution of cladding mechanical properties. Additionally, the paper explores how these findings could inform the development of a t@T threshold for cladding integrity and concludes with a gap analysis that identifies areas for future research.

2. Example Cladding Temperature Conditions during an AOO

A parametric study using the TRACG model of the Edwin I. Hatch Nuclear Power Plant (Hatch) Unit 2 was conducted to evaluate post-DO parameters, such as peak cladding temperature (PCT), peak heatup

rate, and the duration of time in DO for a typically limiting AOO event. This analysis aims to help identify the potential operational envelope for extending AOO operation to include DO analysis but does not intend to constrain or require the analyzed envelope in future core licensing evaluations.

Hatch Unit 2 is a BWR/4 located in Southeast Georgia and operated by Southern Nuclear, utilizing GNF3 10×10 fuel [20]. A licensing model of Cycle 29 was used as a reference case to simulate a turbine trip with no bypass (TTNBP) and no end of cycle recirculation pump trip (RPTOOS) event and a feedwater controller failure (FWCF) – High Demand event, which are both typically limiting AOOs for the plant. Two modeling approaches were used to artificially worsen the reference licensing model results. A range of hot channel power peaking factors (HCPPFs) were applied to perturb the reference licensing model and induce a CPR < 1.0 during the transient. This approach artificially increases the bundle power during the event beyond the reference model, thereby worsening the CPR response. The results of this perturbation are shown in Figure 1. Separately, a range of CPR multipliers were applied to reduce the calculated CPR from the reference licensing model without impacting bundle power distribution. This method artificially lowers the critical power calculated from the licensed CPR correlation, thereby resulting in predicted bundle powers that are closer to the DO condition relative to the reference case. The results of this perturbation are shown in Figure 1. In the perturbations, DO times were calculated as the maximum of either a) the amount of time where CPR < 1.0 or b) the amount of time between when CPR first drops below 1.0 and the time at which PCT begins to decrease (from rewetting).

A combination of these effects would be expected in a core design that credits limited DO for licensing. Firstly, core designs would take advantage of the additional CPR margin and seek to lower bundle CPRs. This would be partially obtained by reducing core reload batch sizes, which would tend to concentrate power into fewer, higher-power bundles. Both of those modeling approaches were taken in order to determine whether post-DO behavior significantly differs between these effects.

As evidenced by the results in Figure 1, DO occurs as the HCPPF increases from 1 to 1.15, although the calculated duration of DO is extremely short (~0.15 s). The calculated heating rate is quite high (~300–400°C/s), causing the cladding temperature to rise by approximately 60–120°C during this brief DO. Increasing the HCPPF further to 1.2 results in DO lasting longer (~1s). Longer durations of DO naturally lead to higher PCTs with increased heating rates. The HCPPF = 1.2 scenario represents a reasonable condition for the expected cladding performance regime, with a pre-transient MCPR > 1.20 (the non-perturbed case initial CPR was 1.49).

As evidenced by the results in Figure 1, DO duration increases as the predicted CPR is scaled from 1 to 0.5, although the calculated PCTs and heatup rate are less severe. The calculated heating rate for CPR multipliers of 0.6 and 0.5 are on the order of ~500–650°C/s, causing the cladding temperature to rise by approximately 150–200°C during this brief dryout (<1.3 s). The CPR multiplier of 0.6 scenario represents a reasonable condition for the expected cladding performance regime, with a pre-transient MCPR > 1.18 (the non-perturbed case initial CPR was 1.49). This initial pre-transient MCPR is similar to the case described above with the HCPPF = 1.2. These two cases are comparable with the case that has a higher channel power (HCPPF = 1.2), resulting in a higher heatup rate and maximum PCT as expected.

Based on these results, the post-t@T transient operational envelope can be defined as a scenario where the heating rate is approximately 650°C/s to 800°C/s, the PCT reaches around 550°C, and the temperature is sustained for just over 1 s. This configuration keeps the cladding well under the alpha–beta phase transition temperature for zirconium-based alloys. However, these temperature regimes may be high enough to impact irradiation hardening and as-fabricated residual cold working, alter predefined microstructures, and affect second phase particle (SPP) size and distribution within the material; they may also be high enough cause the cladding to exceed the yield stress.

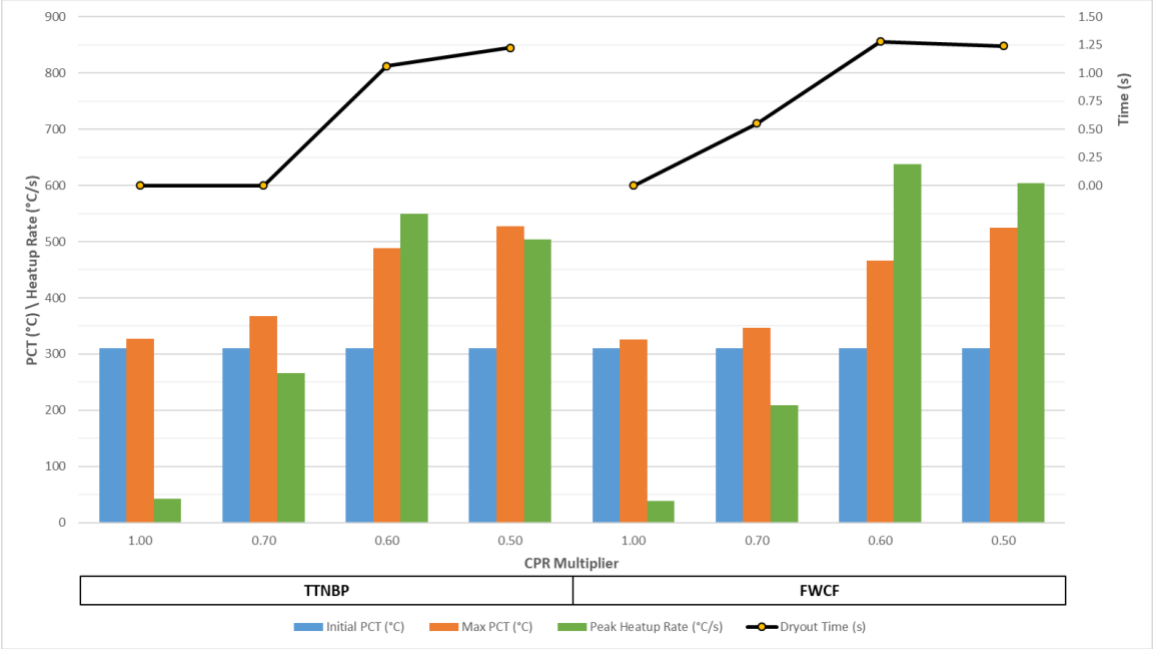

Figure 1. Plant Hatch Turbine Trip with No Bypass (TTNBP) [21] and Feedwater Controller Failure (FWCF) CPR Sensitivity Evaluation focusing on PCT, Heatup Rate and DO Duration

PWRs are typically constrained by Class IV transients, such as locked rotor events. Currently, there is no publicly available analysis that defines the expected temperatures, heating rates, and duration at temperature for these conditions. PWR AOOs are generally considered more aggressive than their BWR counterparts. Therefore, conducting such an analysis for PWRs would provide valuable insights into the expected operating conditions. However, it is important to note that results may vary depending on the specific PWR design and vendor assembly. Fortunately, a post-t@T experiment conducted at the University of Wisconsin-Madison [22] offers some relevant data. The results indicate that under simulated PWR AOO conditions following CHF, cladding temperatures are likely to range from 525°C to 850°C and potentially reach a maximum temperature of 1000°C, and these temperatures can persist for up to 6 seconds. Reaching these temperatures would place the cladding well within the alpha–beta transition zone, or potentially even fully in the beta regime. If the cladding temperature does reach these temperatures, significant microstructural changes could occur, along with higher oxidation rates and hydrogen uptake. Although it may be unrealistic to assume that the cladding could return to service following such an event, these changes do not necessarily imply cladding failure or excessive brittleness. Demonstrating the structural integrity and mechanical properties of the cladding after such an event could provide valuable data for refining dose consequence analysis.

3. Zircaloy Phenomenon Occurring during a Rapid Temperature Transient

The evolved microstructure of the cladding during operation prior to rapid transient is briefly described here to illustrate the expected mechanical behavior under rapid transients. During operation, multiple degradation mechanisms affect cladding microstructure. The major mechanisms considered here are irradiation damage, corrosion, and hydrogen effects (hydriding). The effect of the irradiation damage corresponds to irradiation hardening of the cladding due to the increase of the number density of irradiation-induced defects. These defects act as barriers to dislocation motion, which increases the flow stress. Major defects are <a> or <c> component dislocation loops, either interstitial or vacancy in character, and precipitate amorphization or dissolution occurs under irradiation [5-8]. The dissolved elements, such as Fe from $Zr(Fe,Cr)_2$ or $Zr(Fe,Ni)_2$ or Zr_2Fe/Ni, are associated with <c> component

dislocation loops [9]. A similar phenomenon occurs for Nb-bearing alloys, where Nb preferentially precipitates at <c> loops. Oxide layer formation is commonly considered non-load-bearing, so its impact on mechanical behavior is limited to the reduction of wall thickness.

During a rapid transient, the local oxide layer thickness at the affected region may increase, which could initiate a localized surface defect during cooling. Hydriding affects mechanical behavior in several ways, including delayed hydride cracking [10,11], embrittlement caused by unfavored hydride microstructure and reduced deformability at high hydrogen concentrations [12-17], and altered thermal creep rates [18]. For no-liner BWR cladding, the estimated overall hydrogen content at limiting transients (i.e., ~30 GWd/MTU or less) is expected to be around 200 wt. ppm and is expected to dissolve completely during a transient; in contrast, lined BWR cladding can have hydrogen concentrations above 1000 wt. ppm at high burnups [19]. Depending on the temperature and hydrogen content during a rapid temperature transient, the thermal creep rates can increase due to hydrogen-enhanced localized plasticity mechanisms. As cooling starts, dissolved hydrogen re-precipitates according to the cooling rate profile; the final hydride microstructure can affect ductility if unfavorable hydride features are present in the cladding. Hydrogen pick-up is considered to be negligible due to the duration of the transient.

4. Zircaloy Performance under Transient Annealing Conditions

The performance of Zircaloy, particularly its mechanical behavior and corrosion resistance, has been extensively studied since its adoption for nuclear applications. The interest in removing DO and DNB as a failure metric for Zircaloy under AOOs and reactivity initiated accidents (RIAs) is growing and has generated a renewed focus on Zircaloy performance following transient annealing conditions—termed t@T, as mentioned previously—in order to inform licensing methodologies. Two key figures of merit are relevant to t@T applications. The first is the impact of thermal transients on the post-transient mechanical performance. Thermal transients induce changes in the microstructure of Zircaloy that then affect its mechanical properties. These microstructural changes are primarily driven by the recovery of irradiation-induced defects and recrystallization processes. These phenomena are expected to reduce the yield and ultimate tensile strength of the cladding while increasing both uniform and total elongation. Additionally, thermal and possibly irradiation-induced creep may become more pronounced compared to the pre-transient state. However, following the transient, irradiation hardening resumes, which shifts the mechanical properties of the material back toward their pre-transient conditions. These changes in the microstructure following the transient do not mean that the cladding will regain its pre-transient state, and they also do not indicate whether the rod has failed or will fail. Instead, a licensee will need to incorporate these changes into their respective methodology and assess how these changes impact subsequent operation.

The second figure of merit concerns the impact of thermal transients on the post-transient corrosion behavior of the cladding. Like mechanical behavior, this characteristic is influenced by microstructural changes, particularly those involving the redistribution and growth of SPPs in the material. SPPs are deliberately introduced through heat treatments during fabrication to enhance the cladding's resistance to oxidation and hydrogen pickup. Alterations in the size or concentration of these SPPs during a thermal transient can potentially lead to increased oxidation and hydrogen uptake, both of which are known to contribute to failures in various accident scenarios (e.g., loss-of-coolant accidents, RIAs, and fuel handling accidents) [40]. Although understanding the redistribution and growth of SPPs during an AOO transient are crucial, this manuscript focuses primarily on the mechanical performance of Zircaloy.

The mechanical performance of cladding is typically assessed by measuring properties such as hardness, yield stress, and ultimate tensile stress. However, comparing these properties across different datasets (e.g., hardness vs. yield stress) and materials (e.g., Zircaloy-2 vs. Zircaloy-4) can be challenging due to inherent differences in material properties, measurement techniques, and material compositions. Therefore, it is necessary to organize the data in a way that normalizes the changes in mechanical properties so that a direct comparison of the variations across different material types and conditions can

be performed. In this context, the goal is to compare how the mechanical properties change relative to the thermal transient conditions (i.e., heating rate, duration, and maximum temperature). To better understand the relationship between these post-transient changes and the material's pre-transient and fully annealed or recrystallized behavior, the following proportional relationship for recrystallization [25-27] was modified and applied:

$$F = \frac{MP_m - MP_a}{MP_i - MP_a}. \quad (1)$$

In Eq. (1), MP_i represents the initial mechanical property of the material prior to a thermal transient. For example, it could be irradiated or unirradiated material. MP_a corresponds to the expected lower bound of the mechanical property measured after the transient, and MP_m is the measured mechanical property following the transient. MP_a was defined based on the fully annealed condition of the material. In all referenced studies, a data point is reported in which the material was fully annealed at an elevated temperature (approximately 700 °C) for about one hour. Where such a condition was not explicitly documented, the condition with the highest annealing temperature and longest hold time was considered representative of the fully annealed state. The outcome of this analysis yields a factor F, which ranges between 0 and 1. In some cases, F may exceed 1 as a result of a lack of statistical testing and the presence of unreported uncertainties and errors in the experimental test data. However, if sufficient statistical data are available, the value of F, minus its associated uncertainties, will generally be ≤ 1. It is important to note that this method requires certain assumptions, as the data acquired from the literature may not always have been intended for this specific application. For instance, when a material property is not measured prior to the thermal transient, MP_i will be taken from the lowest temperature transient available in the dataset. Similarly, MP_a is theoretically one of two values: either the as-fabricated mechanical property representing the annealing of all irradiation defects or the fully annealed mechanical property representing a fully recrystallized microstructure. In this case, MP_a was selected from the highest temperature transient in the available datasets. This approach is designed primarily to normalize the data for comparison across different conditions. A more detailed discussion on the best practices for applying this method in fuel performance applications is provided later in the manuscript.

4.1. Parameters Influencing Zircaloy Performance Post-t@T Transient

Much of the existing research on the impact of thermal transients on Zircaloy performance has concentrated on evaluating the annealing of irradiation-induced defects and recrystallization [1-36]. The material data used in these studies are sourced from publicly available datasets that encompass both unirradiated and irradiated Zircaloy-2 and Zircaloy-4. Unirradiated Zircaloy-2 materials are classified into two categories: standard recrystallized annealed (RXA) material and RXA material that has undergone either 50% or 80% cold work (CW). The CW being introduced to simulate the introduction of irradiation defects and dislocation loops. The irradiated Zircaloy-2 materials are all RXA, some of which are specifically noted as having a liner. One study included hardness testing on the pure zirconium liner [31]. Zircaloy-4 samples were exclusively cold-worked, stress-relieved (CWSR), although some unirradiated data are available for Zircaloy-4 subjected to 30% CW and annealing treatment prior to testing. Sauby et al. [34] performed tests on Zircaloy-2 material with four different oxidation concentrations to assess the impact of oxygen on the material behavior response. There is no publicly available literature on advanced or niobium-bearing Zircaloy alloys (e.g., ZIRLO, Opt. ZIRLO, or M5). In terms of testing methods, most samples were heated using induction heating, and a single thermocouple was used to monitor the temperature. The exception to this setup was the samples tested in the Halden BWR [35,36], which were exposed to AOO heating conditions. While other heating methods may have been employed in some studies, the induction heating method was used in the majority of tests.

Any new material criteria intended to replace the existing DO/DNB criteria must account for the full range of relevant parameters, including both the transient conditions and the material's state prior to the

transient. The transient itself involves three key factors: (1) heating rate, (2) maximum temperature, and (3) duration at temperature. The material properties are more complex but can be categorized into two primary aspects: the as-fabricated material and the accumulated fluence. It is important to note that the types of defects accumulated during irradiation depend on temperature. However, in LWR claddings, the temperature is well-defined and remains constant. Therefore, temperature effects can be excluded from further consideration. An independent t@T criterion would need to incorporate a more detailed analysis of the as-fabricated material, taking into account factors such as heat treatment and alloy composition. However, a fuel vendor could eliminate this consideration by developing a specific criterion for their various Zircaloy cladding concepts.

The initial analysis examined the impact of a simple heat-up and cool-down transient, where the time at temperature was effectively instantaneous. This approach involved using an induction heater to rapidly heat the samples to a target temperature under atmospheric conditions. The samples were then quenched to stabilize the microstructure and prevent any further changes. Figure 2 shows a few examples of these heating conditions for a range of heating rates from approximately 1°C/s to 100°C/s. The primary goal of the study was to assess the effect of the thermal transient on the material microstructure by measuring the change in hardness prior to and following the transient. The proportional factor from Eq. (1) was then plotted as a function of terminal temperature to identify the temperature at which the mechanical performance of the cladding begins to be adversely affected.

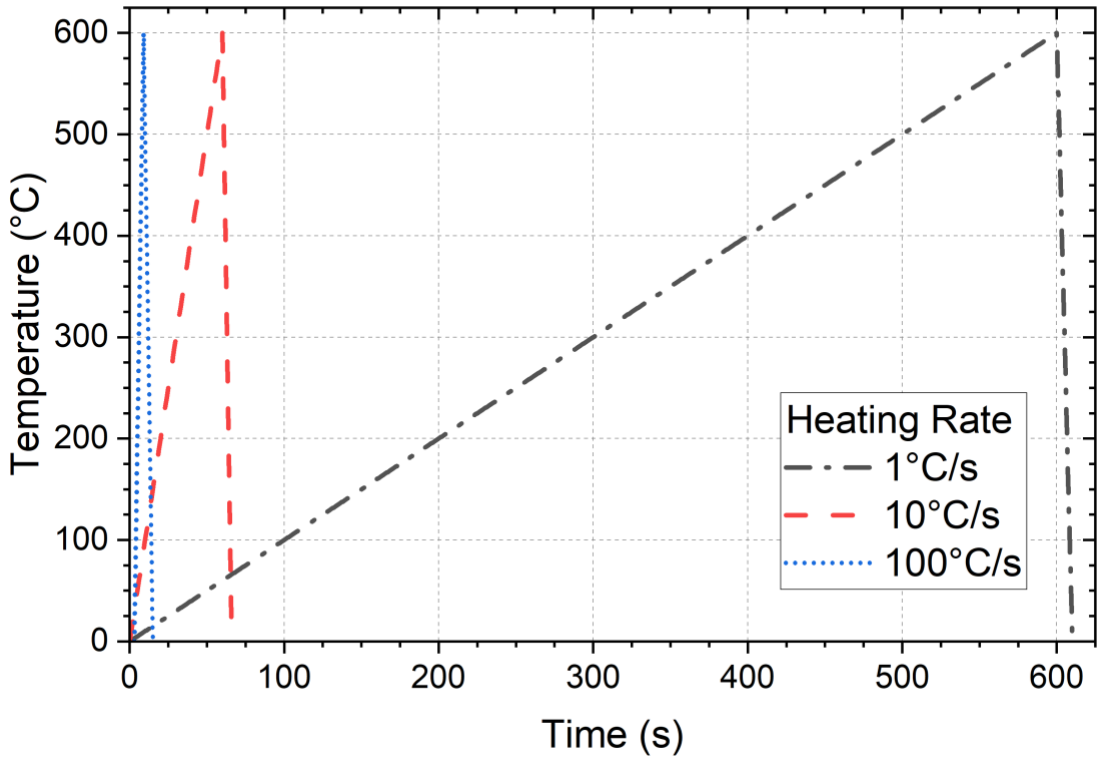

Figure 2. Example temperature and heating rate conditions used to assess the changes to the Zircaloy recrystallization factor for an instantaneous temperature transient.

Figure 3 summarizes the change in the proportional factor calculated from unirradiated Zircaloy-4 hardness data as a function of temperature following a thermal transient with no hold time at temperature.

A detailed analysis of the data suggests that it can be categorized by slow, medium, and fast heating rates. The figure plots data points grouped according to three distinct heating rates: <0.5°C/s, 5–28°C/s, and >100°C/s. The first observation is a clear dependence on the heating rate. Both recrystallization and annealing are time- and temperature-dependent processes. A slower heating rate allows more time at temperature up to the terminal point, which thus allows for more time for dislocation mobility, annihilation of dislocations alongside nucleation and growth of recrystallized grains. In contrast, there is less time at temperature at higher heating rates, which limits recovery and recrystallization. This kinetic suppression of these mechanisms can lead to retained deformation substructures or inhomogeneous grain growth after quenching. While there is a noticeable distinction between the 5–28°C/s and >100°C/s heating rates, the statistical resolution between these two groups remains unclear. Further statistical analysis may be necessary to define a clear demarcation line. However, given that AOOs in both BWRs and PWRs experience heating rates around 200°C/s, the >100°C/s data set offers a reasonable representation of the transient conditions expected during such events.

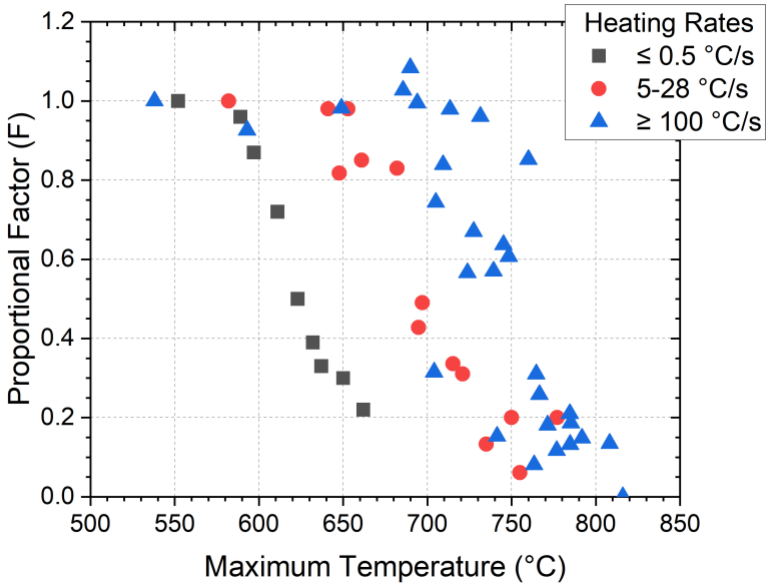

Figure 3. Proportional factor for unirradiated Zircaloy-4 generated from hardness data as a function of heating rate and maximum temperature [1,27,30].

Figure 3, specifically the >100°C/s heating rate data, suggests an upper boundary condition for cladding mechanical behavior changes around 700°C–750°C. However, AOOs inherently involve a time component during the period at temperature. Figure 4 builds on the data from Figure 3 by incorporating and analyzing this time component. The data from Figure 3 is represented in Figure 4 as the <1 s data (black squares). Note that the <1°C/s data is excluded, as it is considered outside the relevant conditions for an AOO transient. The remaining data, for hold times greater than 1 second, are new in Figure 4. The key observation here is the clear effect of time at temperature on the cladding proportional factor. The cladding mechanical response begins to decrease at lower temperatures when the hold time increases to 5 s. However, there are insufficient data to pinpoint the exact temperature at which material properties begin to change. The data suggest the cladding is either fully recrystallized or annealed at temperatures above 650°C, with the cladding being in a partially transformed state around 650°C. At times longer than 15 s, the cladding appears to be fully recrystallized or annealed at 600°C, and no further changes in hardness are observed below 600°C. Lastly, there were insufficient data to make this comparison for Zircaloy-2 or to make a comparison between Zircaloy-4 and Zircaloy-2.

AOO conditions are rapid events that typically last between 3 and 5 seconds; however, spent fuel drying involves lower cladding temperatures (<500°C) and longer hold times (~hours). These differing conditions require a more detailed look at the data and possibly a breakdown of the data by long and short hold times. The data shown in Figure 4 are broken up by material type; Figure 4a represents unirradiated Zircaloy-4, and Figure 4b represents unirradiated Zircaloy-2 with CW of either 50% or 80%. The proportional factor results in Figure 4a suggest, for short hold times, an upper bound temperature of around 700°C (possibly up to 750°C) for time intervals of <1 s when the cladding hardness is fully impacted. The lower bound temperature for cladding changes in the proportional factor appears to be around 600°C.

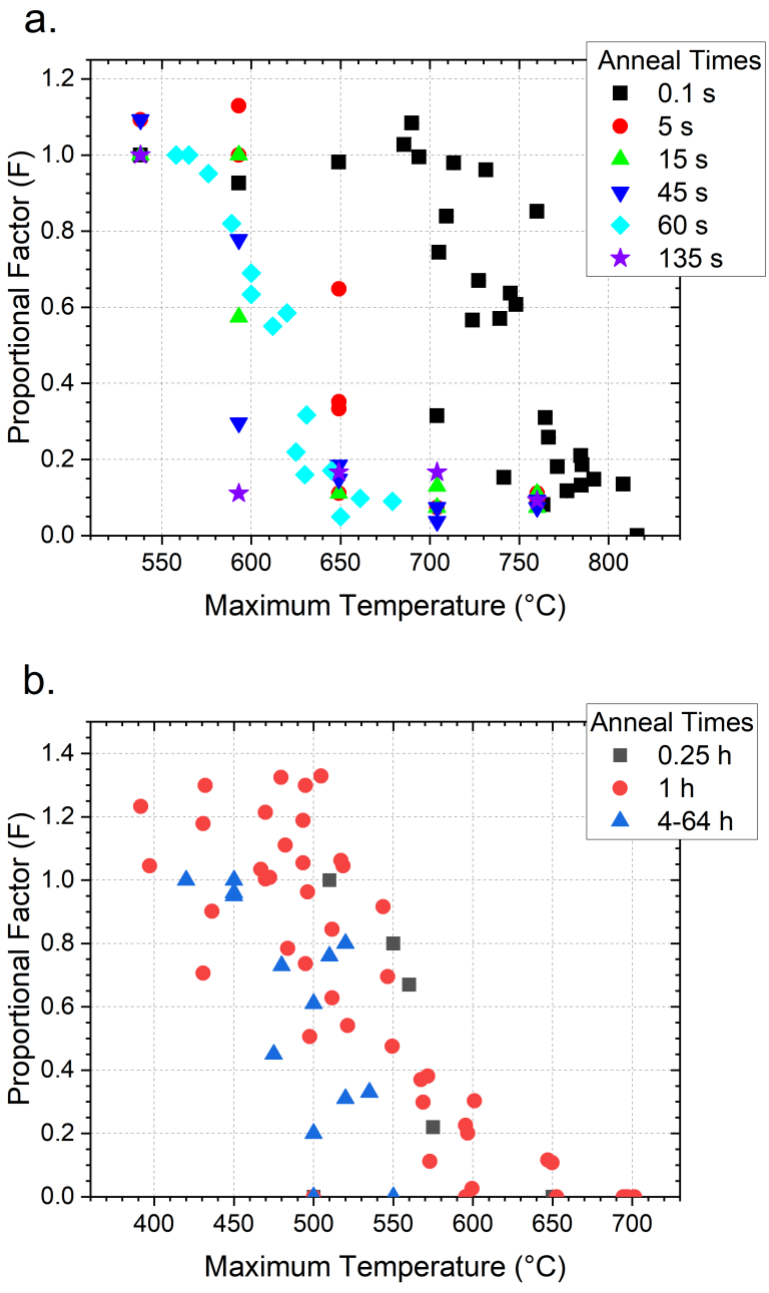

Figure 4. Unirradiated proportional factor for a) Zircaloy-4 and b) Zircaloy-2 generated from hardness data as a function of hold time and max temperature [1-34].

As previously discussed, two possible mechanisms could have driven the observed change: recrystallization or dislocation annealing. The data shown thus far reflect only the change in the mechanical response but do not explain which mechanism governs the observed change. Determining the phenomenon responsible for this change requires detailed microstructural analysis, such as electron backscattering diffraction (EBSD) or transmission electron microscopy (TEM), to examine grain size morphology and dislocation loop structures before and after the thermal transient. Hunt et al. [1] thoroughly investigated the microstructural changes on Zircaloy-4 during simulated thermal transients; they used TEM to explore the mechanism responsible for the change in material hardness. They systematically evaluated the microstructure and hardness of a Zircaloy-4 following a transient held at the terminal temperature for 60 seconds. Additionally, they investigated the microstructure of cladding that experienced a transient with a heating rate of 25°C/s, similar to those shown in Figure 2. Hunt's TEM analysis successfully demonstrated that the change in the hardness of the material was directly related to recrystallization rather than recovery. The study also demonstrated that the proportional factor from the hardness data correlated with the measured TEM images for a number of hold times. Additionally, they noted that TEM provided a more accurate representation of the proportional factor, as there were noticeable errors in the measured hardness, particularly after high-temperature transients.

The Zircaloy-2 data in Figure 4b are for noticeably longer hold times (times ≥0.25 hrs), which makes it challenging to directly compare material performance to the Zircaloy-4 data. Nonetheless, the results suggest that material performance under these extended hold conditions is generally comparable. The trend in Figure 4b shows greater scatter than the trends observed in Figure 4a, and the temperatures are slightly lower: the onset of change occurs around 450°C and completes at ~600°C. Additionally, the mechanical properties under these conditions do not show a strong dependence on hold time. Although longer exposures (4–64 hours) at higher temperatures may indicate a slight decrease in the terminal temperature, this trend may reflect a lack of statistical data rather than a true material effect.

Data from Sauby et al. [34] are represented by the 1 h hold time, and the primary variable of interest in the study was the oxygen content in Zircaloy-2. While oxygen was shown to impact the magnitude of the hardness, the analysis shown in Figure 4b indicates that the rate of change between the four variations of Zircaloy-2 remained the same. TEM data do not exist for this dataset to assess the responsible mechanism for the lower temperature changes, but one possible explanation is that the observed changes result from annealing of dislocations induced by the CW. This would suggest that recrystallization has not occurred and that perhaps the observed change in the proportion factor is more representative of irradiation-induced annealing rather than recrystallization.

A comparative analysis is shown in Figure 5, which contrasts the effects of slow heating rates (<1°C/s) with extended hold times (>15s). The resulting changes are nearly identical, suggesting that similar modifications to mechanical performance can occur based on either the heating rate or the hold time—as long as there is sufficient time for recrystallization mechanisms to activate and alter the microstructure.

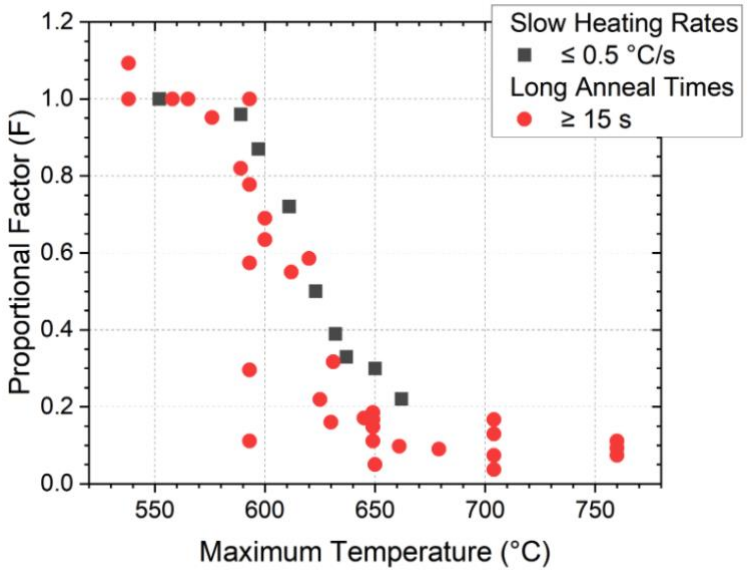

Figure 5. Comparison of the Zircaloy-4 recrystallization factors based on hardness data for long hold times (>15 s) and slow heating rates (<1°C/s) [1,28,30].

The final and potentially more complex assessment concerns the impact of a thermal transient on irradiated materials and their post-transient performance. Irradiation generates point defects, which may evolve into larger defects, such as dislocation loops. This defect propagation leads to an increase in material hardness, thereby affecting both the steady-state and transient performance of the cladding. In addition, irradiation temperature may also be an important parameter to consider [32]. As previously discussed, two primary mechanisms contribute to changes in mechanical performance. During a thermal transient, irradiation-induced defects may be annealed such that the material's mechanical properties may be restored to pre-irradiated levels. Additionally, recrystallization may occur in conjunction with recovery of radiation damage, further complicating the response. It is, therefore, crucial to identify the temperature ranges where these mechanisms are active and to evaluate the transition between them. In some cases, one mechanism may dominate in specific temperature regimes, which would eliminate the need to consider the other phenomenon. To assess this behavior, t@T testing on irradiated Zircaloy-4 and Zircaloy-2 is presented in Figure 6a and Figure 6b, respectively. Two key observations emerge from the data. First, a regression of the proportional limit occurs at lower temperatures, starting around 350–400°C. However, this regression is likely directly related to the extended hold times (ranging from hundreds of seconds to several days). These hold times are significantly longer than those typical of AOO t@T conditions (3–5 s) and those associated with recrystallization (0.1–135 s). The presence of a high concentration of dislocations may lower the recrystallization temperatures. This suggests that the observed change is primarily due to the annealing of irradiation-induced defects. Figure 6b shows two distinct data clusters. The first cluster, spanning temperatures from 225°C to 425°C with hold times of >1000s, strongly suggests that annealing is taking place. The second cluster, which is observed at higher temperatures (~500–625°C) with shorter hold times (~100 s or less), may indicate either annealing or recrystallization. However, due to the lack of microscopy analysis, it is difficult to definitively determine which mechanism predominates in this temperature range.

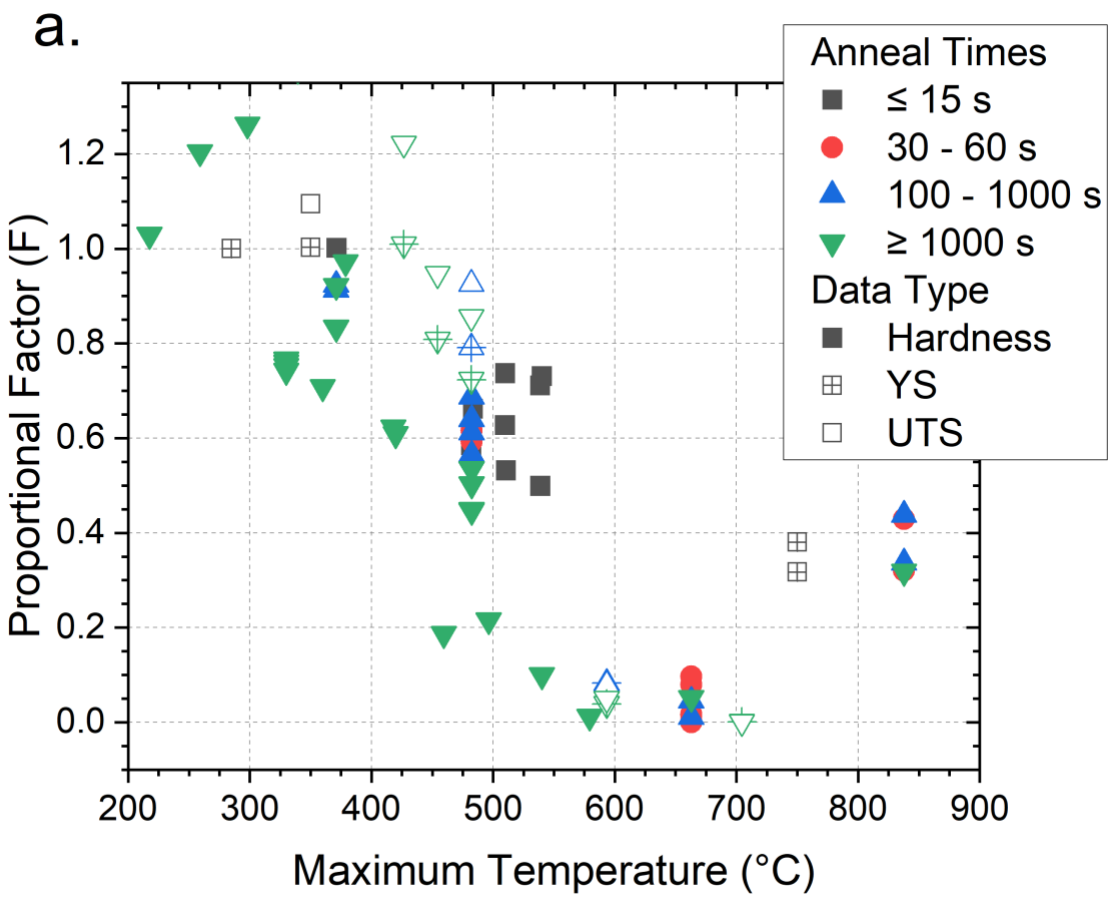
a.
Anneal Times
≤ 15 s
30 - 60 s
100 - 1000 s
≥ 1000 s
Data Type
Hardness
YS
UTS
Proportional Factor (F)
0.0
0.2
0.4
0.6
0.8
1.0
1.2
200
300
400
500
600
700
800
900
Maximum Temperature (°C)

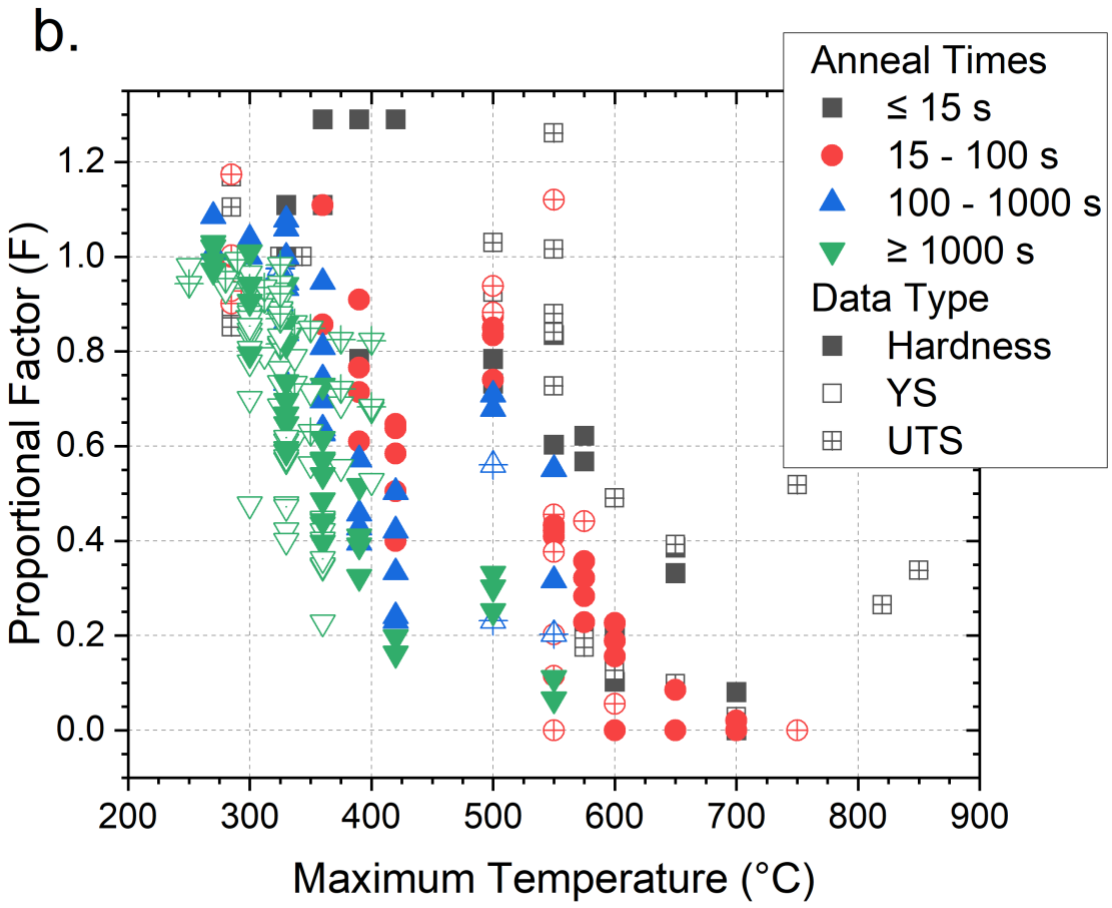

Figure 6. Proportional factor for irradiated a) Zircaloy-4 and b) Zircaloy-2 as a function of hold times [29-32,35-39].

A key parameter to consider is the effect of irradiation temperature on the pre-transient material properties and the subsequent impact on defect annealing during a transient. This has been a primary focus of research for many metals used or considered for nuclear environments. However, this topic has not been as extensively studied in other materials. Notably, Howe et al. [8] investigated this behavior in Zircaloy-2 at two different irradiation temperatures. After irradiation, the samples were subjected to various annealing conditions to assess the influence of irradiation temperature on the annealing rate. The effect was examined in two ways: as a function of annealing temperature for a constant annealing time (Figure 7a) and annealing time at a constant temperature (Figure 7b). In both cases, significant differences were observed in the annealing behavior of the material. The first key observation, shown in Figure 7a, is that samples irradiated at higher temperatures exhibit a slower rate of change in material properties compared to those irradiated at lower temperatures. This difference occurs at higher annealing temperatures. The second observation, shown in Figure 7b, is that samples irradiated at higher temperatures undergo less annealing overall than those irradiated at lower temperatures. A likely explanation for this result is that the higher irradiation temperatures result in a lower density of irradiation-induced defects due to the complex interplay between the generation and irradiation-enhanced diffusion of these defects as a function of temperature. Consequently, there are a lower density of larger defects in the samples irradiated at higher temperatures, leading to smaller changes in material properties during subsequent annealing. In BWRs and PWRs, coolant temperatures during operation are typically around 285°C. However, pressure conditions vary, and this variation leads to different coolant and heat

transfer conditions. As a result, cladding temperatures can range from 300°C to 350°C along the axial length of the fuel rod. These axial temperature variations can influence the mechanical properties of the cladding based on the local irradiation temperature conditions. Following an AOO transient, the mechanical properties of the cladding in regions that are subjected to higher temperatures are likely to be less affected by the transient. However, there is a general lack of data on this behavior, and, therefore, obtaining data to confirm this hypothesis would be valuable, as it could support a deeper understanding of post-transient performance.

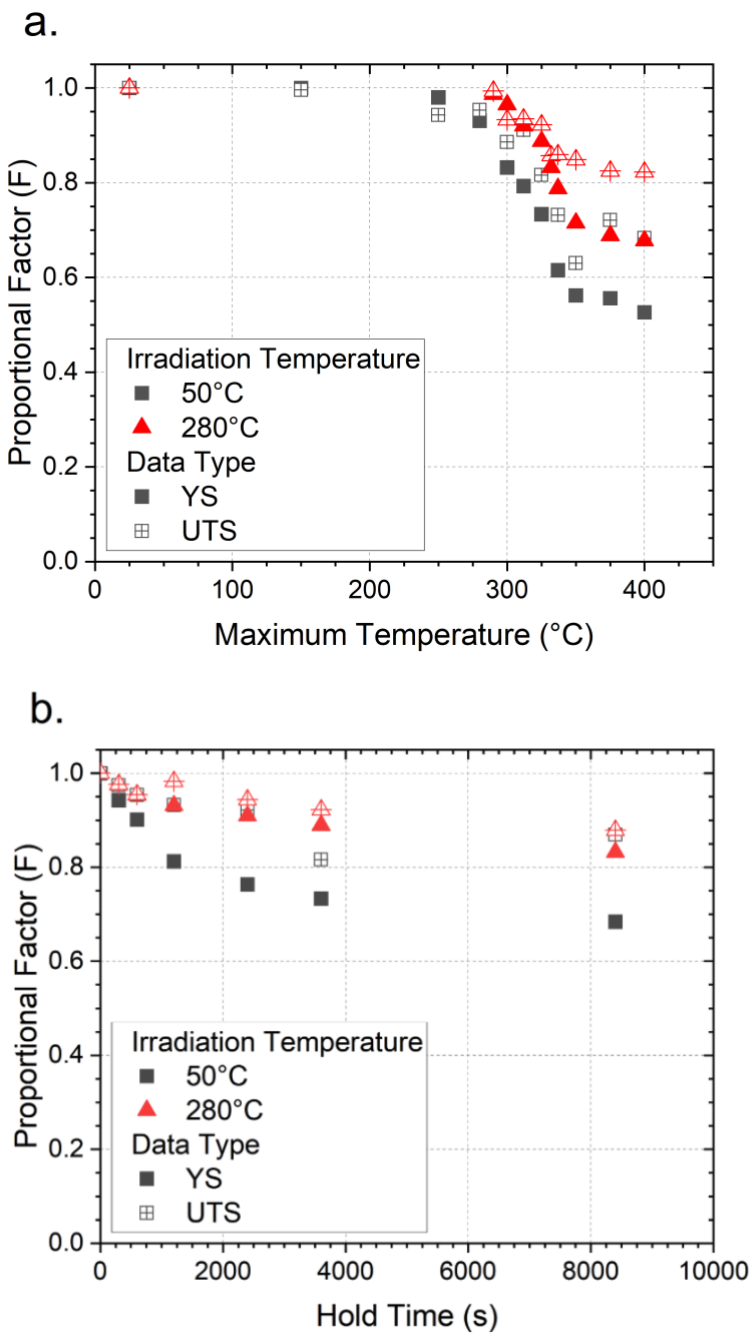

Figure 7. Proportional factor as a function of irradiation temperature with respect to a) annealing temperature and b) annealing time at 325°C [32].

4.2. Machine Learning Analysis of Post Transient Zircaloy Data

The uncertainty inherent in the sparse t@T data prompted the adoption of a robust data analysis approach. This approach included data curation, the use of the Pearson correlation coefficient to assess the strength of linear relationships between features, and Shapley analysis on a machine learning (ML) model to evaluate the impact of features on the target variable, F. The data curation step was performed on the dataset shown in Figure 8 as follows.

Features →

Entries ↓

	Reference	Material	Initial Condition	Cold Work (%)	Oxygen content (ppm)	Irradiation Temperature (°C)	Test Material	Maximum Temperature (°C)	Hold Time (s)	Heating Rate (°C/s)	Hardness (HV)	YS (MPa)	UTS (MPa)	F	Fluence x 10^{24} (#/cm^2)	Burnup (GWd/t)	Neutron displacement damage (dpa)
0	Torimarue	0	0	0.0	350.0	347.0	0	25.000000	0.000000	0.0	150.800000	0.0	0.0	1.000000	2.70	13.5	4.1
1	Torimarue	0	0	0.0	350.0	347.0	0	500.000000	2.123747	40.0	139.500000	0.0	0.0	0.732000	2.70	13.5	4.1
2	Torimarue	0	0	0.0	350.0	347.0	0	500.000000	20.785334	40.0	139.800000	0.0	0.0	0.740000	2.70	13.5	4.1
3	Torimarue	0	0	0.0	350.0	347.0	0	500.000000	75.597019	40.0	144.500000	0.0	0.0	0.850000	2.70	13.5	4.1
4	Torimarue	0	0	0.0	350.0	347.0	0	500.000000	326.601888	40.0	138.500000	0.0	0.0	0.709000	2.70	13.5	4.1
...	...	...	...	...	...	...	...	...	...	...	...	...	...	...	...	...	...
605	Carpenter	3	7	0.0	0.0	50.0	4	417.972350	3600.000000	0.0	227.906977	0.0	0.0	0.622674	0.05	1.0	0.3
606	Carpenter	3	7	0.0	0.0	50.0	4	459.447005	3600.000000	0.0	210.465116	0.0	0.0	0.186628	0.05	1.0	0.3
607	Carpenter	3	7	0.0	0.0	50.0	4	496.313364	3600.000000	0.0	211.627907	0.0	0.0	0.215698	0.05	1.0	0.3
608	Carpenter	3	7	0.0	0.0	50.0	4	540.092166	3600.000000	0.0	206.976744	0.0	0.0	0.099419	0.05	1.0	0.3
609	Carpenter	3	7	0.0	0.0	50.0	4	579.262673	3600.000000	0.0	203.488372	0.0	0.0	0.012209	0.05	1.0	0.3

610 rows × 17 columns

Figure 8. Snapshot of the original dataset.

(i) The text data—such as materials, initial condition, and test material—were mapped as integer values to enable computations. For instance, initial condition was grouped based on the material conditions and references where the material's initial condition was not reported, as shown in Table 1. The same approach was applied to all text data.

Table 1. Example of text data mapping

Initial condition (or reference)	Assigned integers
RXA	0
HWR-666 (reference)	1
Annealed	2
CWSR	3
SRA	4
Lee (reference)	5
Hobson (reference)	6

(ii) Empty data entries were replaced by 0.

(iii) Fluence, burnup, and displacements per atom were treated as separate data features. A conversion factor was applied between these parameters when only one feature entry was available. It was assumed that a fluence value of 10^{22} n/cm^2 for E > 1 MeV corresponds to approximately 15 dpa, based on the LWR core internal components data [41]. To facilitate this approximation, the threshold displacement energies of Fe and Zr were considered to be the same, as outlined in the SPECTER code [42]. The conversion between burnup and fluence, or vice versa, was carried out using linear regression based on known fluence and burnup values.

(iv) Specimens with hardness data collected at the Zr-liner were treated based on the difference in oxygen concentration, assuming an O concentration of 350 ppm. This approach was chosen due to the low variability in material types and tested materials, for which the Spearman correlation analysis yielded insufficient results.

(v) By removing unirradiated data, only irradiated data was also analyzed to check the impact of irradiation parameters such as irradiation temperature and fluence or burnup or primary neutron damage.

The Pearson coefficient method is a widely used approach to determine the strength of features that are linearly related to each other. Pearson correlation coefficients were computed using Eq. (2)

$$r_{x_i x_j} = \frac{(x_i - x_{ave})(x_j - x_{ave})}{\sqrt{\sum_i^n (x_i - x_{ave})^2}\sqrt{\sum_j^n (x_j - x_{ave})^2}}, \quad (2)$$

where $x_{i,j}$ are arbitrary instances of feature pairs such as (Maximum temperature, F) in the t@T data, x_{ave} is the average value of each feature, n is the total number of instances, and r_{xy} are the Pearson correlation coefficients. Absolute values of the coefficients indicate the strength of the linear relation, and the sign indicates the direction of the change. For instance, r_{xy} = +1 or -1 indicates perfect positive and negative linear relation between feature pairs, respectively, whereas the r_{xy} = 0 designates no relationship between those feature pairs. Thus, the values close to +1 or -1 designates stronger feature pair correlations, whereas those close to 0 indicates weak or no relation. Noting that determination of causality between features requires a careful analysis.

Figure 9a and b presents the correlation matrix coefficients for feature pairs in the complete and irradiated only t@T datasets, respectively. Since F is the main parameter of interest, we focused on how other features impacted the F. The first three strong features were circled in Figure 9a and b. The absolute value of the coefficient for maximum temperature with respect to F was greater than 0.5 for both datasets, indicating a strong correlation. Based on the correlation strength scale [43], this suggests that as maximum temperature increased, the F value decreased. This was expected, as recovery or softening tends to reduce the mechanical properties that contribute to the formulation of F. All other features showed weak correlations with F, as the absolute values of their Pearson correlation coefficients were less than 0.3, except heating rate in only irradiated specimen dataset. Overall, results suggested that the maximum temperature during a t@T transient has a more significant impact on fuel cladding performance compared to other features, such as fluence, hold time, and heating rate. The Pearson coefficient matrix also revealed a moderate correlation between maximum temperature and both heating rate and weak correlation with the hold time, suggesting that these factors also influence F. As a result, a detailed analysis was conducted to explore these relationships further.

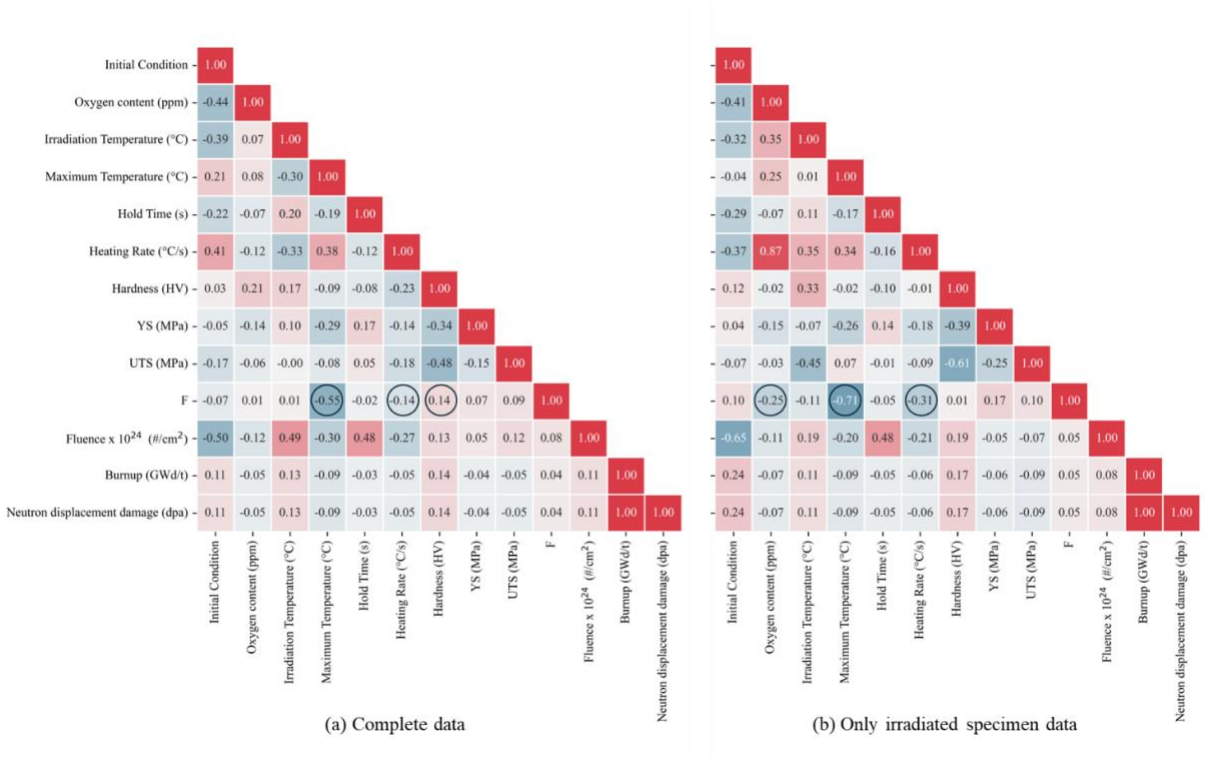

Figure 9. (a) Correlation matrix showing Pearson coefficients of t@T data used in this study and (b) highlighted region of the Pearson matrix.

To further assess the impact of each feature, F was modeled as a function of each feature using supervised ML methods, implemented in scikit-learn [44]. The best-performing ML model was then used for Shapley regression. The ML regression methods included linear regression, stochastic gradient descent, polynomial regression (up to the 6th power), support vector regression, and kernel ridge regression. Grid search was applied to optimize the last two methods. The impact of different scaling options was also investigated. In total, 96 methods (12 regression models and 8 scaling techniques) were tested to identify the model that provided the coefficient of determination (R^2 score) closest to 1 (see Eq. 2). Data splitting was performed randomly, generating training and test sets with sizes of 80% and 20%, respectively:

$$R^2(y, y_p) = 1 - \frac{\sqrt{\sum_i^n (y_i - y_p)^2}}{\sqrt{\sum_i^n (y_i - y_{ave})^2}}, \quad (3)$$

where y_i represents the true F values, and y_p represents the ML-predicted F values. Since F values were derived using metrics relevant to mechanical properties, features such as hardness, yield strength (YS), and ultimate tensile strength (UTS) were excluded from the ML regression to prevent overfitting. Additionally, basic multilayer perceptron (MLP) regression was applied with hidden layers ranging from 20 to 214, using available solvers and activation functions in scikit-learn. Among all the ML regression combinations, the best R^2 score of 0.766 was achieved using kernel ridge regression with grid search and a power transformer. The relatively low R^2 score can be attributed to the high uncertainty inherent in the data.

For the complete dataset, the best R^2 score of 0.79 was achieved using SVR with grid search and a quantile transformer. The relatively low R^2 score was attributed to the high uncertainty inherent in the data. For the irradiated data only dataset, the best R^2 score was 0.88 using SVR with grid search and a

power transformer. This was due to more uniform data structure as compared to complete dataset since all non-rad data was removed to have an impact on the results. The best-performing model, that with the highest R^2 score, was then used to estimate the Shapley regression values using Shapley additive explanations (SHAPs) to assess the feature importance in the ML model [45,46]. For determining the Shapley values, the linear Shapley algorithm was applied [45].

Figure 10 a and b display the SHAP values for complete and irradiated only datasets, respectively, indicating the impact of each feature on the model. In general, features with SHAP values near 0 have minimal or weak effects on the F value. As the SHAP values deviate from 0, the impact of those features on F becomes more pronounced. According to the SHAP values, the maximum temperature had the highest impact on the model's prediction of F, consistent with the results from the Pearson correlation matrix. The hold time was the second most influential feature. For irradiated only dataset, the maximum temperature and hold time were the critical features while other features clustered around a SHAP value of 0, suggesting minimal or weak contributions to the determination of F. Surprisingly, the SHAP values indicated that the initial condition of the cladding or irradiation damage had little to no impact on F both datasets.

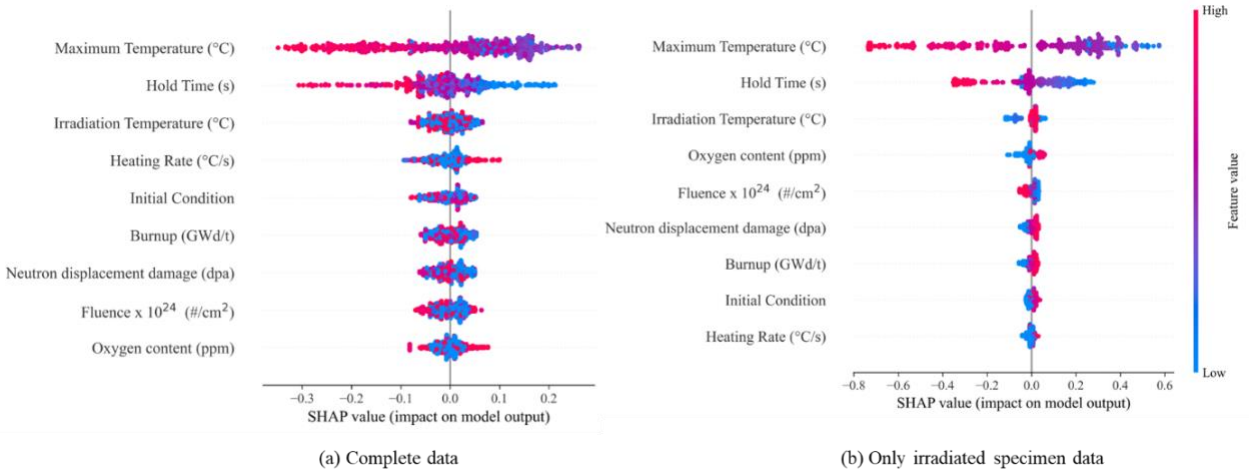

Figure 10. SHAP values of the t@T for (a) complete and (b) only irradiated specimen dataset features in the ML model. Color contours depicted value of feature on the model

Figure 11 presents the mean SHAP values, illustrating the average impact of features on the model's prediction of F. As expected, the maximum temperature had the highest average impact on F, followed by hold time. All other features had little to no impact on F. Assuming any variations were not due to dataset quality, the t@T transients, as well as softening and recovery, were likely influenced more by the maximum temperature and hold time. For irradiated data only, there effects on the F parameter was significantly higher.

It is important to note that the dataset available in the literature was incomplete. Therefore, it is recommended that well-designed experiments on well-characterized specimens, preferably using pre-pilgered rods, be conducted to generate a high-quality dataset. Additionally, further studies on cladding tubes would be valuable.

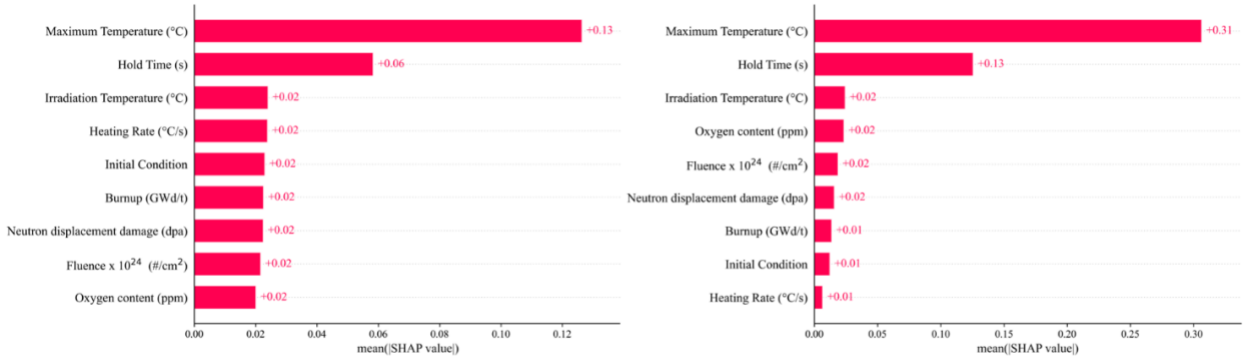

Figure 11. Average SHAP values of the t@T for (a) complete and (b) only irradiated specimen data features in the ML model.

5. Proposed Time-at-Temperature Criteria for Zircaloy Mechanical Performance

Torimaru et al. [31] investigated the irradiation annealing of recrystallized Zircaloy-2 material that had been irradiated to a fluence of 2.7×10^{21} n/cm². The irradiated material was then subjected to a simulated BWR AOO transient, after which the UTS at 343°C and the hardness were measured. The resulting data were fitted using the least squares method to develop an expression for assessing the time–temperature relationship (i.e., t@T) required to anneal out the irradiation defects, where t represents the hold time in seconds and T is the maximum temperature in kelvin.

$$F(T) = \exp\left(-(Kt)^{0.5}\right)$$

$$K = 2.24e11 \exp\left(-\frac{2.09e5}{8.314 * T}\right)$$

This model can be superimposed onto the data presented in Figure 6 to evaluate how well it correlates with a large experimental dataset. It is worth noting that other models have been developed that may be equally applicable [32,39]. However, these models primarily focused on low temperatures and extended annealing times, which are consistent with spent fuel applications. Future work should aim to develop a comprehensive model that bridges the gap between spent fuel applications and short-duration transients. The comparison of the Torimaru to the experimental data is shown in Figure 12 for both Zircaloy-4 and Zircaloy-2. The comparison of the irradiation annealing model with the Zircaloy-4 data is presented in Figure 12a, and the hold time data range from approximately <5 s to 3 h. The model considered only a 100 s hold time, and the model generally fits the data fairly well relative to the experimental data. However, some scatter was observed in the longer hold times; therefore, there would be value in collecting additional data under known conditions to better explain this observation. Figure 12b presents a comparison of the model with irradiated recrystallized-annealed Zircaloy-2 data. The model predicts the behavior for both 1 s, 1 h, and 100 h hold times, which are consistent with the majority of the reported data. As shown, the model calculations effectively fit the data in the lower temperature range (<500°C). However, the model appears not to capture the behavior in the higher temperature regime as well, which generally corresponds to hold times shorter than approximately 100 s. This behavior warrants further investigation and may result from recrystallization or another mechanism not captured by the current model.

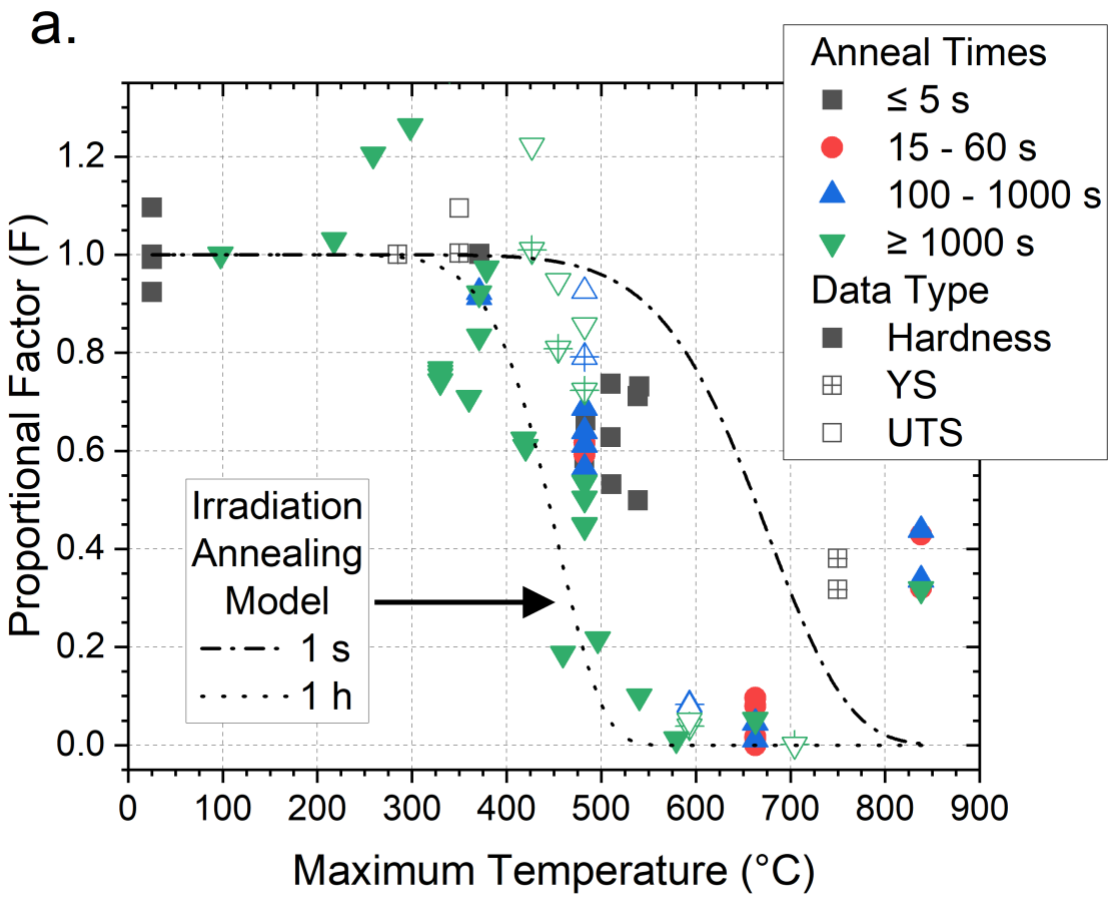
a.
Anneal Times
≤ 5 s
15 - 60 s
100 - 1000 s
≥ 1000 s
Data Type
Hardness
YS
UTS
Irradiation Annealing Model
1 s
1 h
Proportional Factor (F)
Maximum Temperature (°C)
0.0
0.2
0.4
0.6
0.8
1.0
1.2
0
100
200
300
400
500
600
700
800
900

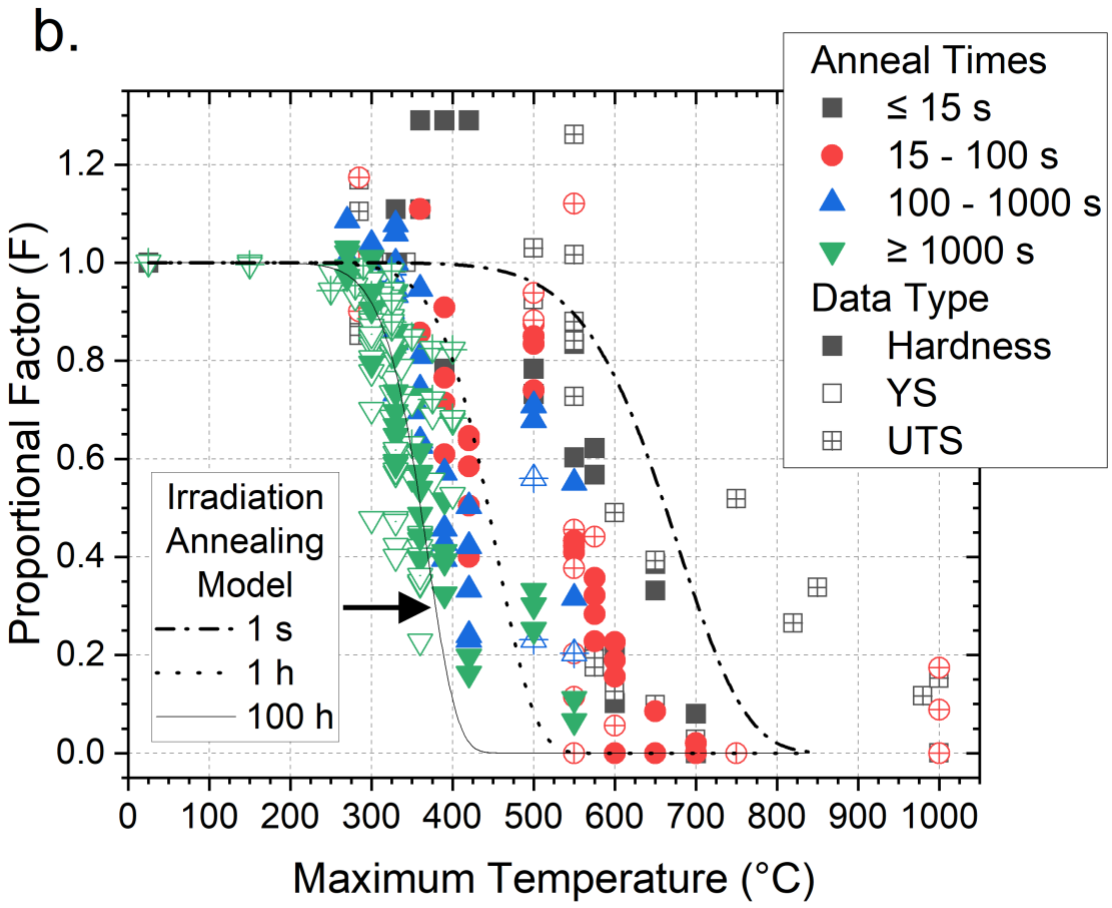

Figure 12. Comparison of the irradiation annealing model to the a) Zircaloy-4 and b) Zircaloy-2 irradiation data for various hold times.

Recrystallization is fundamentally a diffusion-controlled process, and Hunt et al. applied a first-order rate equation to model the data [1,27]. This rate equation typically assumes a constant temperature; however, when applying it to t@T conditions, it is important to account for the effects of both the heating rate and the quenching rate on the resulting microstructure. These factors introduce a time-dependent temperature component, which can be expressed in the following form:

$$\frac{dF}{dt} = \lambda_o exp\left(-\frac{Q}{KT(t)}\right),$$

where λ₀ is a material-specific constant, Q is the activation energy required to initiate recrystallization, K is molar gas constant (8.314 J/mol-K), and T(t) represents the material's temperature at a given time. AOO transients can lead to complex temperature and heating rate profiles in the cladding. However, the process can be simplified into three distinct phases: the heat-up phase is defined by

$$T(t) = T_o + \alpha t, \qquad 0 < t < t_1.$$

Incorporating T(t) into equation 1 yields the following:

$$F(T,\alpha,t) = -\frac{\lambda_o}{\alpha K}\left(QE\left(\frac{-Q}{K(T_o+\alpha t)}\right) + K(T_o+\alpha t)\exp\left(\frac{-Q}{K(T_o+\alpha t)}\right)\right).$$

The isothermal phase is defined by

$$T(T) = T_1, \qquad t_1 < t < t_2.$$

And incorporating T(t) into Eq. (1) yields the following equation for the isothermal phase of an AOO transient:

$$F(T,t) = F_o exp\left(-\lambda_o t exp\left(-\frac{Q}{KT}\right)\right).$$

Lastly, the quench phase is defined by

$$T = T_2 + \beta(t_3 - t) \qquad t_2 < t < t_3,$$

where α and β represent the heating and quenching rates experienced by the cladding, respectively. By integrating Eq. (1) as a function of time, the resulting expression can be written in terms of temperature, heating rate, time, and quench rate as follows:

$$F(T,\mathrm{t},\beta) = -\frac{\lambda_o}{\beta K}(QE\left(\frac{-Q}{K(\beta(t_2 - t_3) - T_2)}\right) + K(\beta(t_2 - t_3) - T_2)\exp\left(\frac{-Q}{K(\beta(t_2 - t_3) - T_2)}\right))$$

where *t* represents the time at a given hold, either at an intermediate or terminal temperature, and F_o is the uncrystallized fraction. Typically, F_o is assumed to be 1, unless the cladding has been heat-treated to induce a partially recrystallized structure, as is the case with more advanced Zircaloy alloys. E(x) is the exponential integral, defined by the following equation:

$$E(u) = \int \frac{exp(u)}{u} du\,.$$

A comparison of F(T,α,t,β) requires both input conditions and an iterative solver, such as a fuel performance code. Many applications of this model will involve heating rates on the order of 200°C/s. At these heating and cooling rates, the impact on recrystallization behavior is minimal, suggesting that the isothermal response may sufficiently capture the material's behavior without accounting for transient effects. Hunt et al. demonstrated the model's applicability to varying heating rates of 0.5°C/s and 25°C/s. Following that approach, the isothermal component in Eq. (2) was considered the available hold times of comparative data from Figure 4, and the results are shown in Figure 13. Figure 13a compares the model to the Zircaloy-4 data and shows good agreement with the hold time datasets. However, the comparison with the 5 s dataset suggests that the model may be somewhat less conservative. It is important to note that data for the 5 s hold time is limited, and, therefore, additional data are needed for a more comprehensive assessment. Lastly, for the <0.5 s hold time data, it would be more appropriate to apply the transient components of the model. While the isothermal model can capture this behavior, doing so requires certain assumptions to be made. The model is also compared to the Zircaloy-2 data in Figure 13b, which feature notably longer hold times (>0.25 hours) as compared to the Zircaloy-4 data. The model was evaluated for hold times of 0.25 h and 1 h, respectively. For a 0.25 h hold time, the model accurately predicts the rate of change in the material properties. At a 1 h hold time, the model provides a reasonable prediction for the rate of change as well. Together, the Zircaloy-4 and -2 comparison suggests that the recrystallization model offers a fairly accurate prediction of changes in material properties. However, the model may not be applicable when applied to modern Zircaloy cladding materials with varying heat treatments. As such, a heat treatment parameter will need to be incorporated into the model as relevant data becomes available.

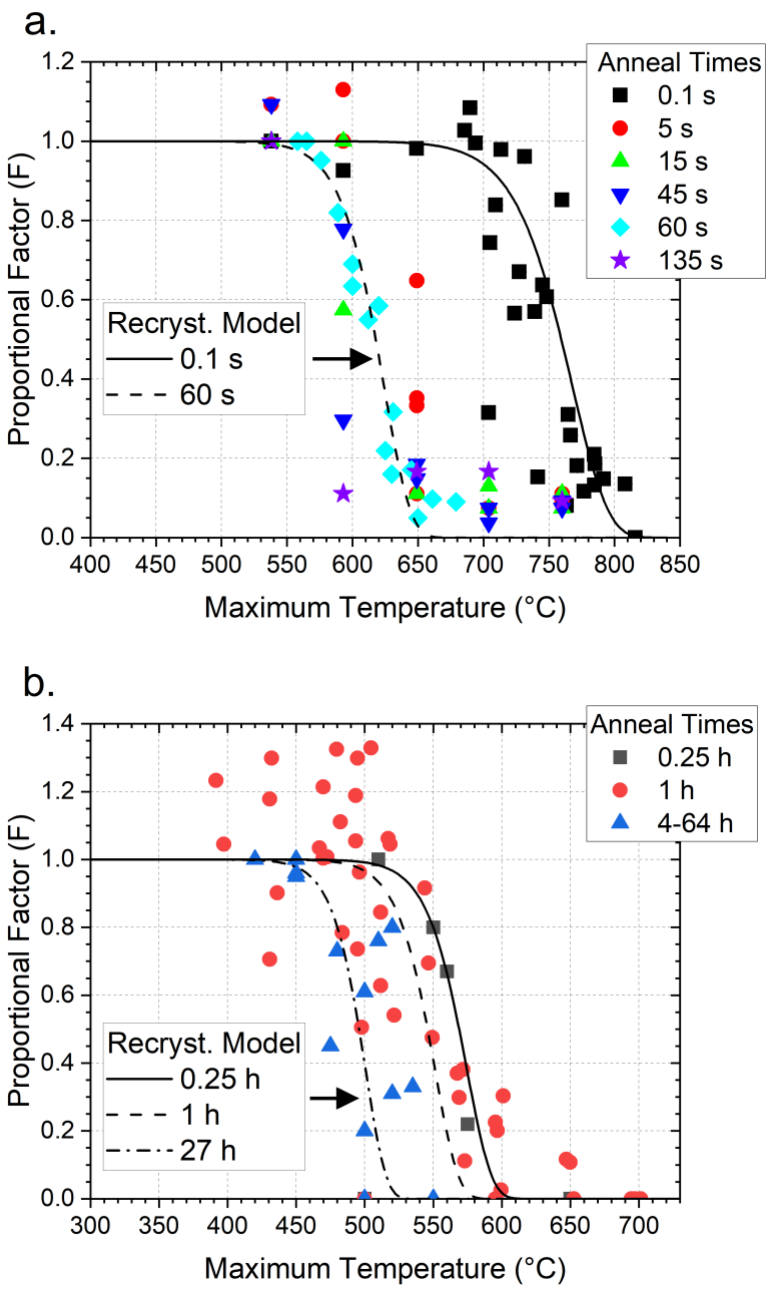

Figure 13. Isothermal model for various hold times compared to the representative recrystallization factor.

Up to this point, irradiation annealing and recrystallization have been discussed separately based on empirical models fitted to experimental data. However, to accurately capture the changes in material properties during an AOO event, both phenomena must be integrated into a comprehensive t@T analysis. Irradiation annealing is a lower-temperature process that theoretically precedes recrystallization [5-8]. Therefore, in developing a unified model, it is logical to start with irradiation annealing. Before an AOO event, the material will have undergone neutron irradiation, likely reaching a saturated state. If irradiation annealing is the only phenomenon considered, then the theoretical lower limit of the material's mechanical properties would correspond to the as-fabricated state. Consequently, irradiation annealing

can be calculated using the model described earlier. From there, the equation for the proportional factor can be applied to estimate the mechanical properties (e.g., hardness, UTS, or YS) resulting from irradiation annealing:

$$F_{irr.\ ann.} = \frac{MP_m - MP_{as\ fab.}}{MP_i - MP_{as\ fab.}},$$

where MP_m is the material property following an AOO transient, MP_i is the pre-transient mechanical property, *and* $MP_{as\ fab.}$ refers to the as-fabricated state of the material properties. As temperature increases, the exponent in the recrystallization model results in an increase in recrystallization, potentially triggering changes in the material's microstructure. In the irradiated state, the material has already undergone irradiation annealing before recrystallization, so the pre-transient material property should account for the effects of this annealing on the material properties. Additionally, the theoretical lower limit of the material's mechanical properties must be defined. In this case, the theoretical limit corresponds to the material's microstructure in a fully annealed state. The recrystallization model can then be applied to calculate the proportional factor, which, in turn, can be used to compute the total change in the mechanical property, as defined by

$$F_{recry.} = \frac{MP_m - MP_{ann.}}{MP_i * F_{irr.\ ann.} - MP_{ann.}},$$

where MP_m represents the material property following an AOO transient, MP_i is the pre-transient mechanical property, and $MP_{ann.}$ refers to the material properties in the fully annealed state. A key modification is the inclusion of $F_{irr.\ ann.}$, which accounts for changes induced by irradiation annealing. The equation can then be refined to calculate the final mechanical property of the material after an AOO transient, as follows:

$$MP_m = F_{recry.} * (MP_i * F_{irr.ann.} - MP_{ann.}) + MP_{ann.}$$

MP_m can then be used in vendor or best-estimate methodologies to assess the impact of changes in mechanical properties on the potential for reusing the fuel following an AOO transient.

6. Conclusion and Future Experimental Data Needs

A substantial body of public literature is available on CWSR Zircaloy-4 and RXA Zircaloy-2, and it includes data with various materials with pre-transient work hardening or annealing. Much of this research focuses on irradiation annealing and recrystallization during simulated thermal transients. The majority of the data examines the evolution of hardness and microstructure in both irradiated and unirradiated Zircaloy as a function of heating rate and hold time. Irradiated data typically involve longer hold times, exceeding 100 s for Zircaloy-4 and 0.25 h or more for Zircaloy-2. In contrast, the unirradiated data primarily address recrystallization in relation to heating rate and hold time. Some studies have investigated pre-transient work hardening and annealing, but no significant differences were observed in the rate of change in material behavior. Collectively, this body of work suggests that it may be possible to develop a t@T criterion for incorporation into fuel performance codes to assess both irradiation annealing and recrystallization. This criterion could help evaluate how these phenomena modify the hardness, UTS, and YS of Zircaloy following an AOO transient. However, several data and modeling gaps remain, preventing the immediate application of this criterion for licensing purposes.

This paper provides a basic analytical comparison of historical cladding alloys, but additional work is required to validate the proposed criterion. Several key data gaps remain that must be addressed to build confidence in the model and improve its accuracy for licensing purposes. Table 2 summarizes these data

gaps and outlines the additional data needed to enhance the model's validity. A significant observation is the general lack of mechanical test data (both unirradiated and irradiated) under highly controlled conditions to validate the proportional factor described in this paper. Of particular importance is the definition of MP_a—particularly in relation to irradiation annealing or recrystallization—as this is crucial for understanding the changes in mechanical properties following an AOO transient. More detailed investigations are needed to define the time and temperature regimes at which irradiation annealing and recrystallization begin to occur. Such work would help refine our understanding of the onset and transition of these phenomena. Howe et al. [32] studied the impact of irradiation temperature on post-irradiation annealing behavior, using samples irradiated at 50°C and 280°C annealing temperatures. Their findings suggest that increasing irradiation temperature may raise the temperature at which irradiation defects are annealed. However, the materials used in previous studies may not be directly applicable to modern cladding alloys such as M5, Optimized ZIRLO, or AXIOM. Therefore, new data are required to either confirm similar performance characteristics in these alloys or to develop a more relevant mechanical performance model. While the previous studies may be applicable to SRA Zircaloy-4, RXA Zircaloy-2, and these materials in various CW states, further experimental studies are needed to verify the applicability of these findings to modern cladding alloys.

Table 2. Mechanical data gaps associated with understanding Zircaloy performance after a transient beyond the CHF.

Data Gaps	Materials	Material Property	Temperature Conditions (°C)	Hold Time	Notes
Heat Treatment Effects	Zircaloy-2 - RXA vs. SRA	Mechanical Properties	450–800	<1 to 15 s	Zry-2 data are limited and specific to RXA and CW. A comparison between RXA and SRA is necessary to assess whether there performance is similar or to identify any differences in performance.
Irradiation Temperature Effects	RXA Zircaloy-2	Mechanical Properties	350–800	<1 to 15 s	Data do not exist for operating temperatures (300–350°C). Data are needed to verify the observed behavior.
Impact of Heat Treatment and Irradiation Effects	Advanced zirconium alloys – Nb containing alloys and pRXA	Mechanical Properties	350–800	<1 to 15 s	No available data.
Transition between irradiation annealing and recrystallization	All Zircaloy materials	Mechanical Properties	350–550	1 to 60 min	Data are available, but they primarily focus on either irradiation annealing or recrystallization. Data focused on assessing the overlap between the two mechanisms and how they influence the resulting mechanical changes would be beneficial.
Yield stress at elevated temperatures	All Zircaloy materials	Mechanical Properties	400-alpha-beta transition temperature	-	Modern alloys with RXA microstructure may not recrystallize, and therefore the yield stress at

					temperature may be the limiting condition.
Impact of Alpha + Beta and Beta temperature regimes impact post transient mechanical performance	All Zircaloy materials	Mechanical Properties (embrittlement)	> 800–1000	<1 s to 60 min	Does not apply to the re-use case.
Creep Down	All Zircaloy Materials	Creep	350–800	<1 to 15 s	Local geometry changes in the cladding may increase sensitivity for pellet–cladding interaction and pellet–cladding mechanical interaction type failures.
Post transient creep performance	All Zircaloy materials	Creep	350–800	<1 to 15 s	Changing the mechanical properties impacts creep behavior, but by how much remains unclear.

7. Acknowledgements

This work was supported by the Advanced Fuels Campaign (AFC) of the U.S. Department of Energy, Office of Nuclear Energy. The authors would like to express their gratitude to Caleb Massey and Ian Greenquist of Oak Ridge National Laboratory (ORNL) for their valuable technical feedback. Additionally, we appreciate the review and input from the Time at Temperature Technical Experts Group (TEG), which significantly enhanced the technical content of this manuscript.

Furthermore, this work is being co-radiated with the Nuclear Energy Advanced Modeling and Simulation (NEAMS) program to integrate the model discussed in this paper and to support the development of mechanistic models capable of capturing the phenomena addressed. This close collaboration between the NEAMS program and the experimental community underscores the strategic importance of bridging mechanistic modeling and experimental research.

8. Reference

1. *Standard Review Plan, Chapter 15*. Nuclear Regulatory Commission, USA: 1998. ML070710376.
2. Time-at-Temperature Operation of Light Water Reactors: Survey of Literature, EPRI, Palo Alto, CA, September 2021, 3002022146
3. G. Verdu, M. J. Palomo, A. Escriva e D. Ginestar, “FORSMARKS 1 AND 2 Stability benchmark, Final Problem Specifications”, OECD/NEA Report NEA/NSC/DOC(2001)2, Paris, France, June 2001.
4. Test Matrix for Determining the Impact of Critical Heat Flux on Cladding Material Behavior, EPRI, Palo Alto, CA, December 2024, 3002029354
5. M. Griffiths, A review of microstructure evolution in zirconium alloys during irradiation, Journal of Nuclear Materials 159 (1988) 190-218.
6. R.A. Holt, R.W. Gilbert, 〈c〉 Component dislocations in annealed Zircaloy irradiated at about 570 K, Journal of Nuclear Materials 137(3) (1986) 185-189.
7. F. Onimus, S. Doriot, J.-L. Béchade, Radiation effects in zirconium alloys, Comprehensive nuclear materials 3 (2020) 1-56.
8. M. Griffiths, R.W. Gilbert, G.J.C. Carpenter, Phase instability, decomposition and redistribution of intermetallic precipitates in Zircaloy-2 and -4 during neutron irradiation, Journal of Nuclear Materials 150(1) (1987) 53-66.

9. Y. de Carlan, C. Regnard, M. Griffiths, D. Gilbon, C. Lemaignan, Influence of iron in the nucleation of⟨ c⟩ component dislocation loops in irradiated Zircaloy-4, Zirconium in the Nuclear Industry: Eleventh International Symposium, ASTM International, 1996.
10. C.E. Coleman, D. Hardie, The hydrogen embrittlement of α-zirconium—A review, Journal of the Less Common Metals 11(3) (1966) 168-185.
11. G.A. McRae, C.E. Coleman, Thermodynamics and kinetics of delayed hydride cracking in zirconium alloys: A review, Journal of Nuclear Materials 601 (2024) 155006.
12. M. Billone, T. Burtseva, R. Einziger, Ductile-to-brittle transition temperature for high-burnup cladding alloys exposed to simulated drying-storage conditions, Journal of nuclear materials 433(1-3) (2013) 431-448.
13. M. Nakatsuka, S. Yagnik, M. Limbäck, P. Barbéris, Effect of Hydrides on Mechanical Properties and Failure Morphology of BWR Fuel Cladding at Very High Strain Rate, Zirconium in the Nuclear Industry: 16th International Symposium, ASTM International2012, p. 0.
14. M. Aomi, T. Baba, T. Miyashita, K. Kamimura, T. Yasuda, Y. Shinohara, T. Takeda, Evaluation of hydride reorientation behavior and mechanical properties for high-burnup fuel-cladding tubes in interim dry storage, ASTM International2008.
15. J.B. Bai, N. Ji, D. Gilbon, C. Prioul, D. François, Hydride embrittlement in ZIRCALOY-4 plate: Part II. interaction between the tensile stress and the hydride morphology, Metallurgical and Materials Transactions A 25(6) (1994) 1199-1208.
16. C. Ells, The stress orientation of hydride in zirconium alloys, Journal of Nuclear Materials 35(3) (1970) 306-315.
17. A.T. Motta, L. Capolungo, L.-Q. Chen, M.N. Cinbiz, M.R. Daymond, D.A. Koss, E. Lacroix, G. Pastore, P.-C.A. Simon, M.R. Tonks, B.D. Wirth, M.A. Zikry, Hydrogen in zirconium alloys: A review, Journal of Nuclear Materials 518 (2019) 440-460.
18. N.R. P Bouffioux, Impact of Hydrogen on Plasticity and Creep of Unirradiated Zircaloy-4 Cladding Tubes Zirconium in the Nuclear Industry: Twelfth International Symposium, ASTM International, West Conshohocken, PA, 2000.
19. P. Konarski, C. Cozzo, G. Khvostov, H. Ferroukhi, Modeling of hydrogen behavior in liner claddings Journal of Nuclear Materials 573 (2023) 154125.
20. https://www.nrc.gov/docs/ML2021/ML20211J260.pdf
21. Solis, J., Ivanov, K. N., Sarikaya, B., Olson, A. M., Hunt, K. W., Organisation for Economic Co-Operation and Development, Nuclear Energy Agency - OECD/NEA, Nuclear Science Committee, Committee on Safety of Nuclear Installations, 46, quai Alphonse Le Gallo, 92100 Boulogne Billancourt (France), & US Nuclear Regulatory Commission (United States). (2001). Boiling water reactor turbine trip (TT) benchmark. Volume I: Final Specifications.
22. KAROUTAS, ZESES, et al. "FUEL ROD TIME AT POST-CHF TEMPERATURE DEVELOPMENT FOR PWR AND BWRs." (2024)
23. Hideaki, F. Takanori, K. Yuichiro, S. Hideo and M. Shinya, "BWR Stability Issues in Japan," Science and Technology of Nuclear Installations, Volume 2008, Article ID 358616, 11 pages, Hindawi Publishing Corporation, 2007.
24. Kozlowski, et. al. ""BWR Stability Event Benchmark based on Oskarshamn-2 1999 Feedwater Transient", OECD/NEA report (restricted access), 2012.
25. C.E.L. Hunt, E.M. Schulson, Recrystallization of zircaloy-4 during transient heating, Journal of Nuclear Materials, Volume 92, Issues 2–3, 1980, Pages 184-190, ISSN 0022-3115, https://doi.org/10.1016/0022-3115(80)90101-4

26. D. Lee, Recrystallization and mechanical behavior of Zircaloy-2 tubing, Journal of Nuclear Materials, Volume 37, Issue 2, 1970, Pages 159-170, ISSN 0022-3115, https://doi.org/10.1016/0022-3115(70)90082-6
27. Chaieb, A., Mozzani, N., Ambard, A., Parrot, A., Köster, A., & Crépin, J. (2022). Stress relieved Zircaloy-4 recovery and recrystallization during fast anisothermal transients. *Journal of Nuclear Science and Technology*, *59*(12), 1558–1566. https://doi.org/10.1080/00223131.2022.2076750
28. D. O. Hobson, The effect of thermal transients on the hardness of zircaloy fuel cladding, ORNL/NUREG/TM-26, June, 1976
29. Ito, K., K. Kamimura, and Y. Tsukuda, "Evaluation of irradiation effect on spent fuel cladding creep properties", Proceedings of the 2004 International Meeting on LWR Fuel Performance, Paper 1117, Orlando, Florida Sep. 19-22, 2004
30. Lowry, L. M., J. S. Perrin, and A. A. Bauer. "Tensile and hardness property evaluations of irradiated zircaloy cladding under off-normal and transient conditions." *Irradiation Effects on the Microstructure and Properties of Metals: A Symposium*. No. 611. ASTM International, 1976
31. T. Torimaru, T. Yasuda, M. Nakatsuka, Changes in mechanical properties of irradiated Zircaloy-2 fuel cladding due to short term annealing, Journal of Nuclear Materials, Volume 238, Issues 2–3, 1996, Pages 169-174, ISSN 0022-3115, https://doi.org/10.1016/S0022-3115(96)00451-5
32. Howe, L M. The Annealing of Irradiation Damage in Zircaloy-2 and the Effect of High Temperature Irradiation on the Tensile Properties of Zircaloy-2. Canada: N. p., 1960. Web.
33. J.W.C. Dunlop, Y.J.M. Bréchet, L. Legras, H.S. Zurob, Modelling isothermal and non-isothermal recrystallisation kinetics: Application to Zircaloy-4, Journal of Nuclear Materials, Volume 366, Issues 1–2, 2007, Pages 178-186, ISSN 0022-3115, https://doi.org/10.1016/j.jnucmat.2006.12.074
34. M.E. Sauby, D. Lee, Recovery behavior of cold-worked and quenched Zircaloy with varying oxygen content, Journal of Nuclear Materials, Volume 50, Issue 2, 1974, Pages 175-182, ISSN 0022-3115, https://doi.org/10.1016/0022-3115(74)90154-8
35. T. HARA, S. MIZOKAMI, Y. KUDO, S. KOMURA, Y. NAGATA & S. MOROOKA (2003) Current Status of the Post Boiling Transition Research in Japan, Journal of Nuclear Science and Technology, 40:10, 852-861, DOI: 10.1080/18811248.2003.9715428
36. McGrath, M A, Ruhmann, H, Oberlaender, B C, and Thorshaug, S. *Investigation into the effects of in-pile dry-out transients on Zircaloy fuel cladding as performed in IFA-613.* Norway: N. p., 2001. Web.
37. Carpenter, G. J. C. and Watters, J. F., "Irradiation Damage Recovery in Some Zirconium Alloys," Zirconium in Nuclear Applications, ASTM STP 551, American Society for Testing and Materials, 1974, pp. 400-415.
38. Precipitate Stability in Zircaloy-2, EPRI, Palo Alto, CA, May 1990, NP-684543
39. H. Yokoyama, et al. EFFECTS OF THERMAL ANNEALING ON MECHANICAL PROPERTY AND MICROSTRUCTURE OF BWR SPENT FUEL CLADDING DURING DRY STORAGE, Proceedings of the 20th International Symposium on the Packaging and Transport of Radioactive Materials, Juan-le-Pins, France June 2023
40. Barberis, P., Charquet, D., Ahlberg, E., Simic, N., Lemaignan, C., Wikmark, G., Dahlback, M., Limback, M., Tagtstrom, P., & Lehtinen, B. (2002). Role of the second-phase particles in zirconium binary alloys (pp. p. 33–58). ASTM International.
41. Chopra, O. K. and A. S. Rao (2011). "A review of irradiation effects on LWR core internal materials – Neutron embrittlement." Journal of Nuclear Materials 412(1): 195-208
42. Greenwood, L.R., *The SPECTER Computer Code for Radiation Damage Calculations*. 2013, IAEA: ; International Atomic Energy Agency, International Nuclear Data Committee, Vienna (Austria). Medium: ED; Size: page(s) 18-21.
43. Cohen, J., *Statistical power analysis for the behavioral sciences*. 2013: routledge.
44. Pedregosa, F., et al., *Scikit-learn: Machine Learning in Python.* Journal of machine learning research, 2011. **12**: p. 2825-2830.
45. Chen, H., et al., *Algorithms to estimate Shapley value feature attributions.* Nature Machine Intelligence, 2023. **5**(6): p. 590-601.

46. Lundberg, S.M. and S.-I. Lee, *A Unified Approach to Interpreting Model Predictions*, I. Guyon, et al., Editors. 2017